DOI 10.1007/s11182-021-02440-0
Russian Physics Journal, Vol. 64, No. 6, October, 2021 (Russian Original No. 6, June, 2021)

ELECTROMAGNETIC PROPERTIES OF 3D CARBON-BASED POROUS STRUCTURES IN HIGH FREQUENCY RANGE

E. G. Shashkova, N. I. Valynets, M. I. Demidenko, and O. G. Paddubskaya UDC 621.355

The paper presents the analysis of the electromagnetic response of three-dimensional carbon-based porous structures (carbon foam) in the microwave (26–37 GHz) and terahertz (0.1–1 THz) frequency ranges obtained by chemical vapor deposition using nickel foam as a substrate. Raman spectroscopy and scanning electron microscopy provide the structural investigations of the obtained carbon films based on a nickel frame. It is shown that due to the nickel catalytic properties, the carbon film represents a sandwich structure in the given synthesis conditions, which consists of multilayer graphene and pyrolytic carbon. According to the analysis of the frequency dependences of reflectance and transmittance of carbon foam with a thickness of 1.6 mm and 300–400 μm pore size, these materials provide a 60% absorption in the microwave range and 100% absorption in the terahertz frequency range. Such thin films used as a carbon skeleton in a combination with flexible polymers can be applied as effective flexible absorbers of radiofrequency radiation.

Keywords: graphene, thin carbon films, carbon foam, electromagnetic properties, radiofrequency absorbing materials, shielding coatings.

INTRODUCTION

Unique opportunities, which allow applying the terahertz radiation (0.1–10 THz) in spectroscopy, medicine, biology [1], non-destructive testing, atmospheric monitoring [2], data transmission [3] promote a rapid development of research in this field. Due to a low ionization ability in comparison with microwave and X-ray radiations and relatively high permeability in comparison with the optical radiation, the terahertz frequency range offers fresh prospects for the analysis of biological objects (DNA, RNA, cells, *etc*.) and carrying out high-speed imaging [4]. At the same time, transmittance of most dielectrics (paper, plastic, textile) and high reflectance of metals facilitate the implementation of terahertz technologies in the development of the latest-generation non-destructive testing techniques. Due to the high transmission capacity and weak susceptibility to electromagnetic field fluctuations, the radiofrequency range represents a critical shift in the development of state-of-the-art high-speed data transmission [5], the 5th generation of mobile broadband, in which the data exchange rate can reach 11 Gb/s near 0.2 THz [6].

At the same time, such a rapid development and implementation of terahertz technologies promotes a search for new shielding materials that effectively reduce the growing influence of the electromagnetic interference [7]. Moreover, the development of this field is one of the priority tasks of safe data transmission and protection, which can be solved by many approaches proposed. Thus, the development of carbon materials (graphite, graphene, carbon nanotubes, carbon nano-onions) and composites produced therefrom, is one of the important research fields, which is primarily due to their relatively low cost and a wide spectrum of properties [8]. It is interesting to note that unlike metal shields, in which the electromagnetic shielding is conditioned by reflectance, in carbon-based composites this parameter depends

Research Institute for Nuclear Problems of Belarusian State University, Minsk, Belarus, e-mail: Shashkova.eliz@gmail.com; nadezhda.volynets@gmail.com; demidenko@inp.bsu.by; paddubskaya@ gmail.com. Translated from Izvestiya Vysshikh Uchebnykh Zavedenii, Fizika, No. 6, pp. 76–83, June, 2021. Original article submitted July 20, 2020; revision submitted November 18, 2020.

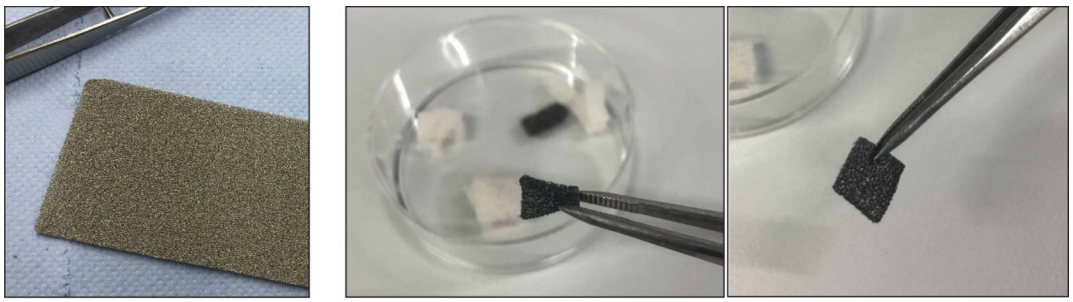

a *b*

Fig. 1. Initial Ni foam (*a*); a mixture of pyrolytic carbon and polydimethyl siloxane (*b*).

on both the reflectance and absorbance. An important limiting factor affecting both the resulting physical properties of composites and their electromagnetic response, is a homogeneous distribution of a carbon filler in dielectric matrices. In this regard, due to the possibility of controlling the internal structure in a combination with such unique properties as low weight, high electrical conductivity, chemical inertness and, most importantly, low cost, carbon foams are a perfect alternative to conventional composites, and have recently attracted particular interest of many researchers.

This work continues previous studies of our research team. In [9–11], we present the experimental results of the electromagnetic response of carbon foams synthesized by carbonification of tannin-containing porous structures and commercial polyurethane foams. The experiments demonstrate a high efficiency of electromagnetic shielding using these materials in a wide frequency range from DC to far infrared range [9], and a possibility of direct control for the electromagnetic response due to changing both the structure (pore size, density) and conductivity of a carbon skeleton [10, 11]. These materials have however a deficiency, namely their mechanical properties, which can be improved through a transfer from a solid carbonic skeleton to a skeleton based on thin carbon films. In this work, we propose such a transfer based on the early obtained data.

As is known, graphene is an atomic-scale hexagonal lattice made of carbon atoms, which has attracted much attention from research teams since been discovered [12, 13]. A combination of optical transparency of 97% in a visible frequency range with high conductivity is used in the production of flexible displays, light-emitting diodes, protective coatings, *etc*. The unique transmission properties of graphene allow using it in terahertz electronics [14]. Batrakov *et al.* [15] first demonstrate the possibility of using graphene/polymer multilayers as an efficient optically transparent and flexible shielding media absorbing 50% of incident radiation in the microwave range. Additional ways to increase the absorption in graphene/polymer multilayers up to 80% are proposed in [16]. From the viewpoint of electromagnetic shielding, thin films based on other graphene-like structures are of interest. For example, pyrolytic carbon (PyC), a disordered structure of amorphous graphene flakes [17]. According to [18], pyrolytic carbon thin films combined with graphene (Gr) reduce the surface conductivity by 2 times allowing to significantly improve the mechanical properties of carbon.

The aim of this work is to consider one the synthesis methods of three-dimensional porous carbon-based (graphene and graphene-like) structures and analyze the effectiveness of the obtained materials in terms of the electromagnetic shielding in the microwave and terahertz frequency ranges.

SYNTHESIS AND ANALYSIS OF THREE-DIMENSIONAL CARBON-BASED POROUS STRUCTURES

Nickel foam 1.6 mm thick presented in Fig. 1*a*, was used for the synthesis of three-dimensional carbon-based porous structures. These structures were cleaned in acetone followed by isopropyl alcohol and then in distilled water prior to synthesis. The specimens were then heated to 80°C for 30 min. It is worth noting that any organic residues on the surface of the metal skeleton could transfer to the amorphous phase in high-temperature conditions, which, in turn could have a negative effect on the mechanical properties and electrical conductivity of the synthesized carbon film. In this regard, the additional specimens on nickel foam were processed in oxygen plasma (Covance plasma source (USA))

TABLE 1. Average Pore Size and Calculated Effective Density of Obtained Carbon-Based Structures

Pore structures	Ni	PDMS	GrPyC/PDMS	PMMA	GrPyC/PMMA
Average pore size, μm	480	370	330	400	330
Density, g/cm^3	0.250	0.104	0.123	0.041	0.044

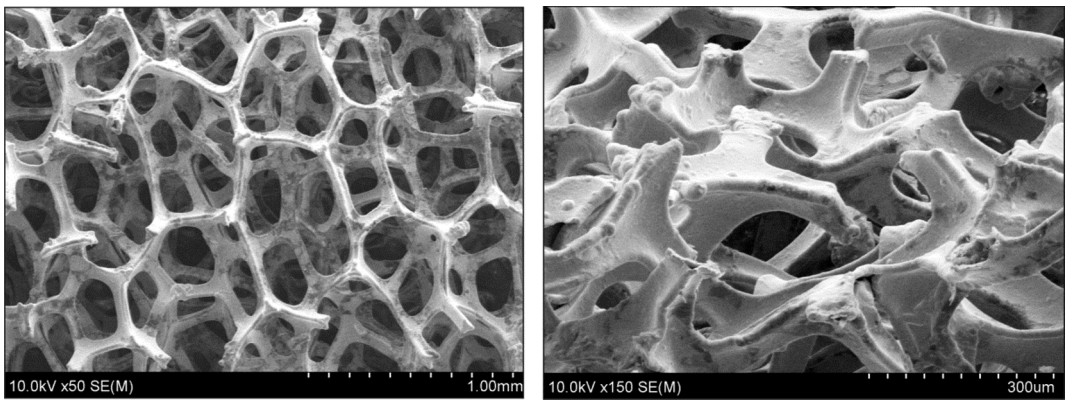

Fig. 2. SEM images of the Ni/GrPyC structure.

at 20 cm^3/min plasma velocity and 100 V for 3 min. Such processing removed organic contaminations, oxide layer, and small roughness on the nickel skeleton surface.

The carbon films (PyC/Gr) were synthesized by chemical vapor deposition (CVD). At the first stage, a 2×2 cm nickel foam specimen was placed in a heat-treating furnace Carbolite Gero (Great Britain). The furnace was then pumped out to 0.06–0.1 mbar pressure and blown with a mixture of nitrogen and hydrogen at a velocity of 60 cm^3/min for an hour. The system was heated up to 1050°C at a rate of 10 degrees per minute in a hydrogen flow (60 cm^3/min). Once this temperature would be reached, it was filled with a mixture of hydrogen and methane in the ratio of 5:20. The synthesis of pyrolytic carbon was performed for 10 min in a static atmosphere. The total pressure in the chamber was 70 mbar. Then the system was cooled down in a hydrogen flow (60 cm^3/min) to room temperature.

The scanning electron microscopy (SEM) images of the CVD-synthesized nickel foam are presented in Fig. 2. The observations are carried out on a Hitachi S-4800 SEM (Japan). One can see that the carbon layer completely covers the initial metal skeleton, but its thickness is not uniform on the skeleton surface.

To improve the mechanical properties of the obtained Ni/GrPyC structure, the specimen surface was reinforced with a thin polymer layer along the skeleton prior to nickel etching. This technique was described in detail in [19, 20]. Two different polymers were used, namely polymethyl methacrylate (PMMA) and polydimethyl siloxane (PDMS). At the first stage, the Ni/GrPyC specimens were placed either in PDMS highly diluted with ethyl acetate (PDMS base, and curing agent and ethyl acetate in the volume ratio of 1:10:100) or in a 6% PMMA solution in anisole. Importantly, in normal conditions, pores in such a structure were filled with air which, in turn, prevented the structure from the polymer penetration, thereby resulting in a nonuniform skeleton coating. To avoid that problem, the specimens were placed in a degassing chamber for 5 min and then dried for the solvent evaporation and the formation of the polymer frame. In the case of PDMS, the processing time was 30 min at 80°C, while in the case of PMMA it was 20 min at 180°C. At the second stage, the Ni/GrPyC/polymer system was put into a 1 M, 50 ml ferric chloride solution for the chemical etching of the Ni skeleton. The obtained GrPyC/PMMA, GrPyC/PDMS structures were washed in distilled water and then dried in air for a day (see Fig. 1*b*). Pure polymer-containing $PDMS_{Ni}$ and $PMMA_{Ni}$ structures were fabricated for comparison. In this case, the initial nickel foam was coated with polymer, and the initial Ni substrate was etched using the technique described above.

The average pore size and the calculated effective density of the obtained carbon-based structures and initial nickel foams are summarized in Table 1. Based on the analysis of these data, the replacement of the metal skeleton by

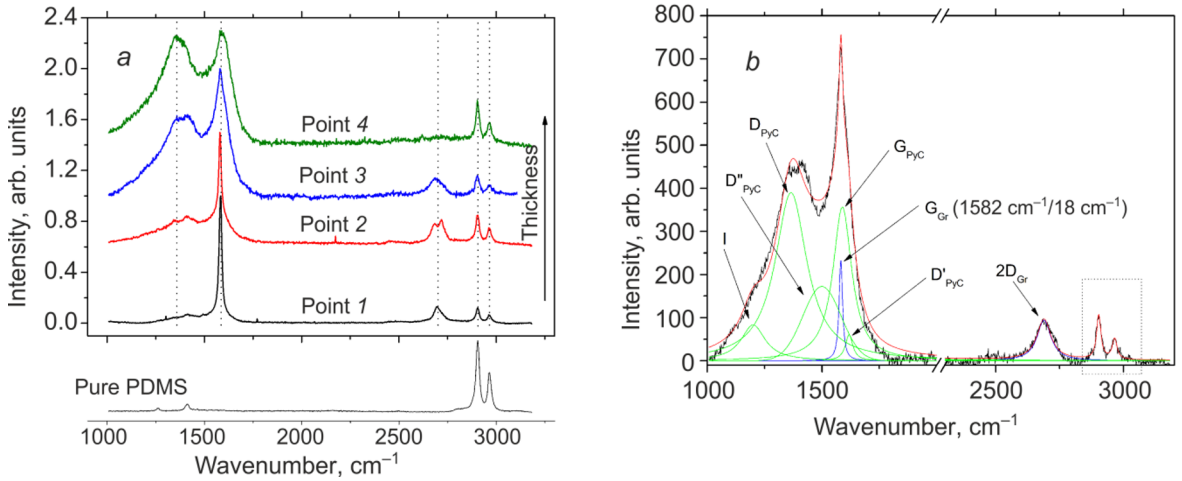

Fig. 3. Raman spectra of GrPyC/PDMS structure: *a* – taken at different points. All spectra are normalized to G band intensity and artificially shifted relative to each other; *b* – spectrum decomposition taken at point *3*, on the Raman line matching the PyC/Gr multilayer contribution.

the carbon skeleton allow to significantly reduce the weight of the obtained materials, i.e., approximately by 2 times for GrPyC/PDMS and 6 times for GrPyC/PMMA structures, the geometry of the metal skeleton being preserved.

The Raman spectroscopy provided additional information about the structure of the obtained materials on a Confocal Raman Microscope Nanofinder HighEnd (Tokyo Instruments, Belarus–Japan) equipped with a 50× objective. Raman scattering was excited by using a 532 nm (600 μW) solid-state laser. The integration time was 30 s to reduce effects associated with the specimen's heating. The Raman spectra presented in Fig. 3, are taken at different points of the carbon frame of the porous GrPyC/PDMS structure.

According to [21–23], the Raman spectra of carbon materials have three characteristic lines. Their analysis shows the presence of one of carbon types. The most intensive are three lines of graphene multilayer corresponding to D, G and 2D bands. The peak at ~1582 cm^{-1} (G band) is caused by in-plane oscillations of sp^2-carbon atoms, *viz*. doubly degenerated phonon mode of E_{2g} symmetry. The full width at half maximum (FWHM) of this peak is ~18–20 cm^{-1}. The peak at 1350 cm^{-1} (D band) is associated with breathing oscillations of the graphene crystal lattice [24]. Since this peak is enabled by the defects, it is called defect. The peak at ~1620 cm^{-1} (D′ band) also refers to the defect type, which is well-pronounced during a transfer from the perfect graphite/graphene structure to disordered structures such as pyrolytic and amorphous carbons [21]. The peak at ~1500 cm^{-1} (D″ band) is often associated with the presence of the amorphous phase. It is important to note that the 2D band (~2690 cm^{-1}) presenting the Raman spectrum indicates to the high crystallinity of graphene structures. The FWHM of the 2D band is a single peak at ~25–35 cm^{-1} observed for one-layer graphene [25]. At the same time, in a multilayer structure, the interaction between layers results in the 2D band broadening and a decrease in its intensity relative to the G band and finally, its decomposition into four separate peaks. In the case of disordered graphene-like structures, this band is not observed.

The obtained carbon films synthesized along the Ni skeleton surface, have a uniform thickness. This is in good agreement with the experimental results of the structure of CVD-synthesized thin PyC films deposited onto copper substrates. Thus, due to a catalytic capacity of nickel from the side adjacent to the skeleton surface, the film structure is graphene multilayer (Fig. 3*a*, point *1*), the whole surface is coated with a PyC layer of different thickness (Fig. 3*a*, points *2–4*). In Fig. 3*b*, we show the Raman spectrum decomposition at point *3* into peaks corresponding to PyC/Gr multilayer.

The analysis of the Raman spectra allows us to estimate the thickness of the obtained carbon layer along the nickel surface. Wang *et al*. [26] report that the penetration depth of 532 nm laser in the carbon layer does not exceed 50 nm. According to the statistical analysis of the Raman spectra, one can note that the greater number of the recorded

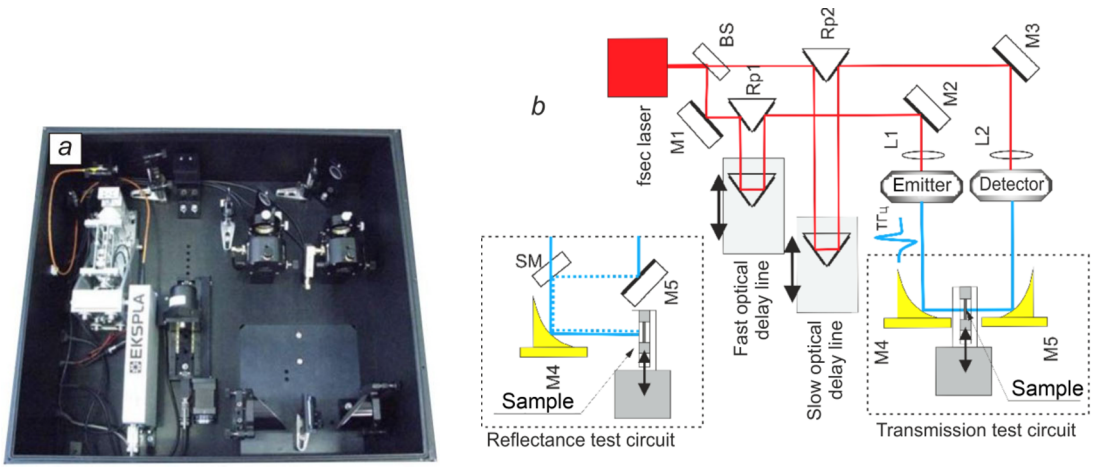

Fig. 4. A photograph of the T-SPEC (*a*) and its optical schematic (*b*). Reflectance (left) and transmittance (right) test circuits. BS – beam-splitter, M1–M5 – parabolic mirrors, Rp1, Rp2 – angle reflectors, SM – semitransmitting mirrors, L1, L2 – focusing lenses.

spectra comprise the peaks matching both pyrolytic carbon and graphene multilayer locating beneath, which, in turn, proves that the average thickness of the carbon film ranges at least from 50 to 80 nm.

It should be noted that the use of PDMS as a reinforcing polymer in conjunction with the low thickness of the carbon layer, provide a sufficient flexibility for the structures synthesized (see Fig. 1*b*). It our research [27] into the PyC/PDMS parallel-sided sandwich structures, we show that this fact plays an important role in the reconstruction of the electromagnetic response of these materials due to their mechanical deformation.

RESULTS AND DISCUSSION

The radiofrequency electromagnetic response of three-dimensional porous carbon-based structures was analyzed in the microwave range 26 to 37 GHz. Real-time T-SPEC Terahertz Spectrometer offered by Ekspla (Lithuania) was used to investigate the electromagnetic response in the terahertz frequency range from 0.1 to 1 THz. Its full view and the optical schematic are illustrated in Fig. 4. At the initial stage, the femtosecond laser pulse of 1050±40 nm wavelength, 40 mW power, and 80 MHz pulse repetition rate, split the incoming pulse in two by a beam-splitter in a proportion of 55:45. The first beam was directed toward the terahertz emitter *via* the fast optical delay line and involved in the terahertz radiation, which, in turn, focused on the specimen by using a system of parabolic mirrors *M*4 and *M*2. Specimens of three-dimensional carbon-based porous structures were placed on a holder normal to the incident radiation. The second beam was used to create a time window on a detector, a signal of which was used to obtain the electric field profile of the terahertz radiation. The discrete Fourier transform was used to convert the terahertz pulse waveform to a frequency spectrum. The additional slow optical delay line allowed broadening the scanning aperture and provided spectral resolution of <5 GHz. The signal-to-noise ratio (over 106:1 at 0.4 THz) was improved by averaging of 1024 measurements. The reflectance was measured by the signal normalizing with the use of the perfect shielding of the terahertz radiation (silica glass plate coated with thin layers of gold).

The frequency dependences of reflectance and transmittance detected in the terahertz frequency range are given in Fig. 5 for $PMMA_{Ni}$, $PDMS_{Ni}$, GrPyC/PMMA, and GrPyC/PDMS structures.

The analysis of these dependences shows that the $PMMA_{Ni}$ specimens are transparent in the terahertz frequency range, i.e., transmittance is 80%. The $PDMS_{Ni}$ specimens demonstrate a significant frequency dispersion, i.e., transmittance drops to zero at 0.6 THz. Such a difference between two polymers in the frequency dispersion can be explained on the one hand, by non-zero dielectric loss tangent of PDMS ($\tan_{PMMA} \sim 0$, $\tan_{PDMS} \sim 0.05$), and on the other

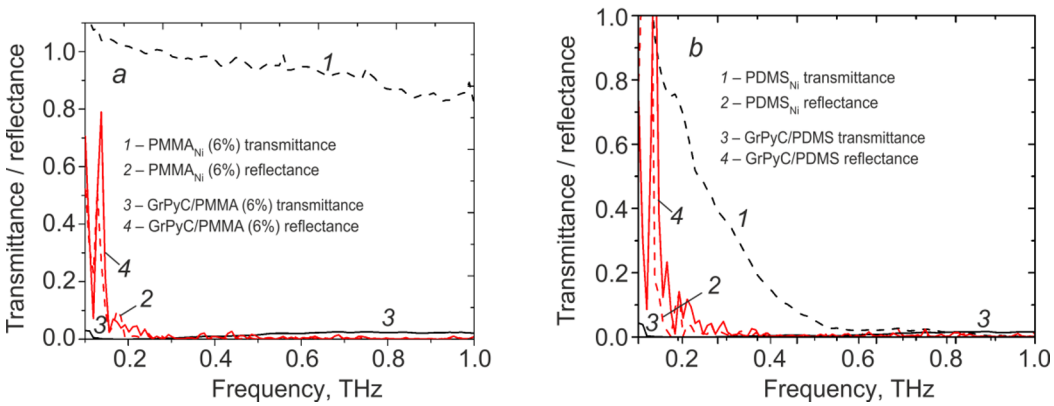

Fig. 5. Frequency dependences of reflectance and transmittance detected in the terahertz frequency range for three-dimensional carbon-based porous structures: *a* – GrPyC/PMMA, *b* – GrPyC/PDMS. The electromagnetic response of pure polymer porous structures is given for comparison. Thickness: 1.6 mm.

hand, by the uniform coating deposition, which has an additional effect on the electromagnetic response of the synthesized materials. We observe that the PMMA coating is more uniform than the PDMS.

In the 0.2–1 terahertz frequency range, the GrPyC/PMMA and GrPyC/PDMS specimens 1.6 mm thick demonstrate zero reflectance and transmittance that indicates a 100% absorption. The initial nickel foams also show zero electromagnetic response in this frequency range (not given in this work). It is worth noting that the measurement technique used for reflectance, in practice determines only the mirror reflection value, while the level of the diffraction scattering remains unknown. According to Table 1, in the 0.2–1 terahertz frequency range, the pore size in such structures is comparable to the wavelength of the incident radiation (1 THz ~ 300 μm), and the diffraction scattering cannot be neglected. Based on the SEM images presented in Fig. 2, we can highlight that the cross dimensions of the nickel skeleton are tens of micrometers. It is therefore easy to estimate that the thickness of the skin layer of the nickel skeleton does not exceed several tens of nanometers in the terahertz frequency range. Thus, we can mostly identify the diffraction of the incident radiation in such structures. In the case of carbon foam, the carbon film thickness is not over 100 nm, which, with regard to the GrPyC conductivity [17, 18], is many times lower than the thickness of the skin layer (~1–10 μm). In our early research [28], we demonstrate that thin PyC films with a thickness of ~70 nm, absorb 50% of the incident radiation. And due to the multiple rereflection, the absorption level can be considerably intensified on the porous geometry of the material skeleton. Based on the results obtained, we suppose that the absorption makes the highest contribution to the electromagnetic response observed in the GrPyC/PMMA and GrPyC/PDMS specimens.

The electromagnetic properties of the specimens in the 26–37.5 GHz frequency range were measured on a R2-408R voltage standing wave ratio and transmission loss meter (Russia) using a waveguide with 7.2 × 3.4 mm cross section. The specimens were placed in a wavegiude perpendicular to the propagation of the electromangetic wave.

The frequency dependences in Fig. 6 are suggested for transmittance and reflectance T and R of PMMA$_{Ni}$, PDMS$_{Ni}$, GrPyC/PMMA, GrPyC/PDMS structures measured in the microwave frequency range of 26–37.5 GHz. Three-dimensional carbon-based porous structures based on pure polymers PMMA$_{Ni}$ and PDMS$_{Ni}$, are transparent in the microwave range, and their contribution to the total electromagnetic response can be neglected, whereas the absorption coefficient $A = 1–T–R$ is 44 and 60% for GrPyC/PMMA and GrPyC/PDMS, respectively at 26 and 37 GHz. This is in good agreement with the experimental data obtained in [9] for the structures with the similar geometry. It is important to note that in the microwave range, the initial nickel foams completely reflect the incident radiation (R = 100%).

The electromagnetic shielding characterization in the microwave range is often based on the value of $SE = -10\log(T)$. It is easy to demonstrate that the GrPyC/PMMA and GrPyC/PDMS structures 1.6 mm thick demonstrate the electromagnetic shielding at a 10 dB level in the microwave range.

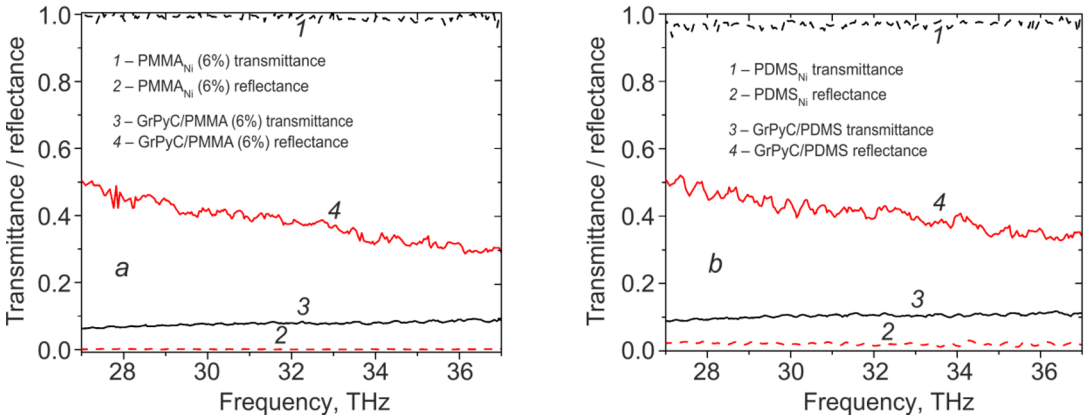

Fig. 6. Frequency dependences of reflectance and transmittance in the microwave range for three-dimensional porous carbon-based structures: *a* – GrPyC/PMMA, *b* – GrPyC/PDMS. The electromagnetic response of pure polymer porous structures is given for comparison. Incident radiation: normal.

CONCLUSIONS

This paper has clearly shown that the carbon-based porous structures are promising materials for the electromagnetic shielding of wide range radiofrequency radiation, namely from the microwave to terahertz frequency range.

The electromagnetic response of such materials was mostly determined by their structure (pore size, skeleton conductively, *etc*.). It was found that a transfer from a solid carbonic skeleton to a skeleton based on thin carbon films with a thickness up to 100 nm in combination with flexible polymers, did not reduce the electromagnetic properties of solid carbon materials and suggested that such materials would be integrated in the up-to-date systems as effective electromagnetic absorber due to its low weight and flexibility.

Further development of the CVD technique applied for the synthesis of thin carbon films will provide varying the conductive properties of the carbon skeleton, thereby creating additional conditions for the development of shielding materials with the reconstruction of their electromagnetic response.

This work was financed by R&D Program “Development of Synthesis Modes and Testing of Multilayer Materials, their Electromagnetic Response and Functional Microwave Irradiation-Transmitting and -Absorbing Modules” in the framework of the Union State ‘Technology-SG’ research line 1.2.1.2 “Development of Integrated Technologies for Developing Materials, Devices and Key Elements of Space Vehicles and Advanced Products for Other Industries”.

REFERENCES

1. D. D. Arnone, C. M. Ciesla, A. Corchia, *et al*., Proc. SPIE, **3828**, 209–219 (1999).
2. P. H. Siegel, IEEE Trans. Microw. Theory Tech., **50**, No. 3, 910–928 (2002).
3. T. Nagatsuma, IEICE Electron. Express, **8,** No. 14, 1127–1142 (2011).
4. M. Beruete and I. Jáuregui-López, Adv. Opt. Mater., **8,** No. 3, 1900721 (2020).
5. M. A. Abdulkadirov and A. P. Semenov, Fotonika, **51**, 62–79 (2015).
6. S. Venkatachalam, D. Bertin, G. Ducournau, *et al*., Carbon, **100**, 158–164 (2016).
7. S. T. Xu, F. Fan, J. Cheng, *et al*., Adv. Opt. Mater., **7**, No. 18, 1900555 (2019).

8. L. Liu, A. Das, and C. M. Megaridis, Carbon, **69**, 1–16 (2014).
9. P. P. Kuzhir, M. Letelier, D. Bychenok, C. *et al*., Russ. Phys. J., **59**, No. 10, 1703–1709 (2017).
10. M. Letellier, J. Macutkevic, P. Kuzhir, *et al*., Carbon, **122**, 217–227 (2017).
11. M. Letellier, J. Macutkevic, D. Bychanok, *et al*., IOP Conf. Ser.: Journal of Physics: Conf. Series, **879**, 012014 (2017).
12. A. K. Geim, Science, **324**, No. 5934, 1530–1534 (2009).
13. A. K. Geim and K. S. Novoselov, Nanosci. Tech., 11–19 (2009).
14. K. S. Novoselov, V. I. Fal'ko, L. Colombo, *et al*., Nature, **490**, No. 7419, 192–200 (2012).
15. K. Batrakov, P. Kuzhir, S. Maksimenko, *et al*., Sci. Rep., **4**, 7191 (2015).
16. K. Batrakov, P. Kuzhir, S. Maksimenko, *et al*., Appl. Phys. Lett., **108**, No. 12, 123101 (2016).
17. N. McEvoy, N. Peltekis, S. Kumar, *et al*., Carbon, **50**, No. 30, 1216–1226 (2012).
18. T. Kaplas and P. Kuzhir, Nanoscale Res. Lett., **11**, No. 1, 1–6 (2016).
19. Z. Chen, Ch. Xu, Ch. Ma, and H.-M. Cheng, Adv. Mater., **25**, No. 9, 1296–1300 (2013).
20. G. Zhou, L. Li, Ch. Ma, *et al*., Nano Energy, **11**, 356–365 (2015).
21. A. Sadezky, H. Muckenhuber, H. Grothe, *et al*., Carbon, **43**, No. 8, 1731–1742 (2005).
22. D. Graf, F. Molitor, K. Ensslin, *et al*., Nano Lett., **7**, No. 2, 238–242 (2007).
23. D. Yoon, H. Moon, H. Cheong, *et al*., J. Korean Phys. Soc., **55,** No. 3, 1299–1303 (2009).
24. A. C. Ferrari, Solid State Commun., **143,** No. 1–2, 47–57 (2007).
25. Y. Hao, Y. Wang, L. Wang, *et al*., Small, **6**, No. 2, 195–200 (2010).
26. Y. Y. Wang, Z. H. Ni, Z. X. Shen, *et al*., Appl. Phys. Lett., **92**, No. 4, 043121 (2008).
27. A. Paddubskaya, M. Demidenko, K. Batrakov, *et al*., Materials, **12**, No. 1, 143 (2019).
28. P. P. Kuzhir, A. G. Paddubskaya, N. I. Valynets, *et al*., J. Nanophotonics, **11**, No. 3, 032504 (2017).